Tunable fulleretic sodalite MOFs: highly efficient and controllable entrapment of C_{60} fullerene via mechanochemistry

Valentina Martinez,[¥[a]] Bahar Karadeniz,[¥,[a]] Nikola Biliškov,[[a]] Ivor Lončarić,[[a]] Senada Muratović,[[a]] Dijana Žilić,[[a]] Stanislav M. Avdoshenko,[[b]] Maria Roslova,[[c]] Alexey A. Popov,*[,[b]] and Krunoslav Užarević *[,[a]]

[a] Ruđer Bošković Institute, 10000 Zagreb, Croatia

[b] Leibniz Institute for Solid State and Materials Research (Leibniz IFW), 01069 Dresden, Germany

[c] Department of Materials and Environmental Chemistry, Stockholm University, Stockholm SE-106 91, Sweden

Keywords: Mechanochemistry, Ball-milling, Fullerene, C_{60}, Metal-organic frameworks, Composite materials, Controllable inclusion, HAADF-STEM

ABSTRACT: Encapsulation and confinement of fullerene guests in metal-organic frameworks (MOFs) lead to a novel class of crystalline fulleretic materials with unique physicochemical properties and a broad field of potential applications. The control over the amount of target guests confined in the MOF structure remains a significant challenge, which is particularly pronounced in the confinement of hardly-accessible fullerene derivatives. The main strategies used in constructing fulleretic composites are limited by the solubility of components used and solvent versus guest competition for inhabitation of the framework voids. As mechanochemical procedures often overcome these issues, we developed here solvent-free processing by ball-milling to gain control over the encapsulation of bulky and rigid C_{60}-fullerene into a sodalite MOF with large cages and narrow cage-apertures. A rapid, green, efficient, and stoichiometry-controlled mechanochemical processing afforded four model C_{60}@ZIF-8 crystalline materials containing target 15, 30, 60, and 100 mol% of fullerene entrapped in the accessible cages of the model sodalite zeolitic-imidazolate framework 8 (ZIF-8), in stark contrast to the solution-based strategies which resulted in almost no loading. Varying the fullerene content affects the framework's vibrational properties, color and luminescence of the composites, and the electron-dose radiation stability. The computational and spectroscopic studies show that the fullerene is accommodated in the cage's center and that the cage-to-cage transport is a hardly feasible and energetically unfavored process. However, the fast release of the C_{60} from ZIF-8 can be effectively controlled by the pH. The entrapment of fullerene molecules in ZIF-8 resulted in their effective isolation even in higher loadings, paving the way to other tunable porous fulleretics containing single-molecule magnets or nanoprobes available on low scales.

INTRODUCTION

Due to their unique molecular structure and electronic properties, buckminsterfullerene (C_{60}) and fullerene derivatives became one of the most important classes of functional materials in the fundamental and applied sciences, such as in molecular electronics[1,2,3], magnetic resonance imaging[4], single-molecule magnetism[5,6], tumor therapy[7], catalysis[8], gas storage,[9] and others. Electron-accepting property, hollow interior, and readiness for functionalization promote their potential application areas, which are especially emphasized in fullerenes functionalized at the exterior or interior side.[10,11] Combination of fullerene's intrinsic properties with the modular structures and chemical properties of metal nodes and walls of porous metal-organic frameworks (MOFs) opens a path towards a novel class of crystalline fulleretic materials with distinctive physicochemical properties and strong potential for application.[12,13] Structurally, MOFs could serve as stable, modular, and versatile matrices,[14–16] enabling spatial distribution and confinement of large guests like fullerenes.[17]

As in other porous materials, the primary strategies for encapsulation[18] of guests into MOFs are the in situ synthesis of the guest inside the cage, in situ growth of the framework in the presence of guests, and post-synthetic absorption (soaking) of guests from the solution. Fullerenes were already considered for post-synthetic inclusion by soaking into MOFs with larger apertures, such as Zn-MOF-177,[14,19] and zirconium DUT-51[20] and NU-901.[21] This strategy, besides requiring an excess of fullerene and a suitable solvent, offers little control in the loading process, and allows the migration and potential egress of fullerene guest.[12,17,22] A particularly exciting example showing limitations in post-synthetic loading is the inclusion of C_{60} in the cobalt-based molecular sponge. The guests populated the channels exclusively, whereas the small cage apertures prevented their inclusion in sizeable M_6L_4 cages.[23] The in situ formation of MOF in a solution containing fullerene was also reported for zirconium-based MOFs, UiO-67,[24] and PCN-222[8]. In all presented cases, the inclusion of fullerene to MOFs was accompanied by the increase in their stability,[25] conductivity,[21] catalytic or photocatalytic properties,[24,26] and has also led to interesting spin structures in these fulleretic materials.[20] However, a general method for the encapsulation of fullerenes into MOFs is still a big challenge due to the low efficiency, solubility of fullerenes, and a need for a large excess of toluene or dichloromethane solvents. Another critical limiting factor is the competition with the solvent for the cage inhabitation, which is particularly emphasized when working with costly and sparse metallofullerenes available at submilligram scales.[27–29]

Recently, mechanochemical reactions, widely used in other fields of materials chemistry,[30–36] have risen as a particularly suitable technique for synthesis, transformation, and functionalization of MOFs,[37–39] with the examples of relevant MOFs as HKUST-1,[40–42] MOF-74,[43,44] zirconium carboxylate MOFs,[45–48] and various zeolitic-imidazolate frameworks (ZIFs).[49–51] Ball milling is best known for avoiding solvation- and solubility-issues, and atom efficiency. It was also used for the encapsulation of discrete organic

molecules.[52–55] Even large flexible guests as enzymes[56] were successfully incorporated into MOFs' cavities by ball milling, enabling a pathway towards MOF biocomposites with improved stability and drug-release time.

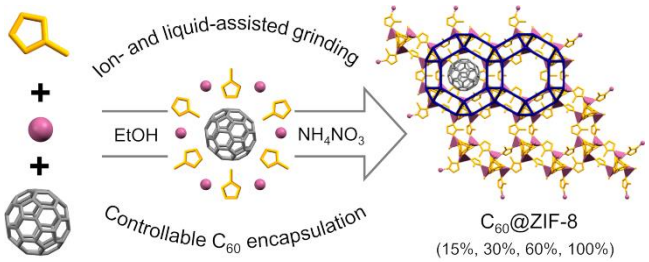

Scheme 1. Schematic representation of the ion- and liquid-assisted grinding procedure for controllable encapsulation of fullerene guests into cavities of ZIF-8. Prepared fulleretic materials contain 15, 30, 60, and 100 mol% of fullerene relative to the maximum theoretical number of voids.

Here we describe a solid-state strategy for controllable encapsulation and immobilization of rigid and bulky buckminsterfullerene C_{60} molecules in the cages of the sodalite phase of ZIF-8[57] by using mechanochemical agitation. The strategy relies on the solid-state templation in a highly efficient and stoichiometry-controlled ion- and liquid-assisted grinding (ILAG)[58] procedure by ball-milling, and using simple, green, and abundant reagents such as ZnO or ethanol. We have successfully prepared four C_{60}@ZIF-8 fulleretic materials with nominal target 15, 30, 60, and 100 mol% of fullerene guests, relative to the number of cages available in the ZIF-8 structure (Scheme 1). This procedure, which is accomplishable at room temperature, is much faster and advantageous before both the solvothermal in situ loading and the post-synthetic soaking approach. The amount of fullerene guests habituating the cages of ZIF-8 has an impact on the vibrational properties of the metal-imidazolate framework and the luminescence of the prepared composites. Computational methods were used to estimate the fullerene's position in the framework and the possibility of fullerene transport through the framework. While the C_{60} immobilized in the sodalite framework remains captured when the composite is sonicated or stirred for a prolonged period, the fast release of the C_{60} is readily accomplished by changing pH. Spectroscopic data revealed that the efficient entrapment of fullerenes enables studies on "single-molecule" fullerene even in composites with a higher loading due to weak interactions of fullerene with other fullerenes or with the MOF walls.

RESULTS AND DISCUSSION

Zeolitic imidazolate frameworks (ZIFs) are a subclass of MOFs formed by imidazole linkers and metal ions characterized by topologies similar to zeolites. Sodalite MOFs with large cages and small cage-apertures are well represented by zeolitic-imidazolate framework-8, ZIF-8.[57] ZIF-8, one of the first commercially available MOFs, is often used, among other applications, for encapsulation of various organic molecules and enzymes for drug delivery and catalysis.[59–62] It was also one of the first MOF synthesized by ball milling.[49] In right milling conditions, ZIF-8 can transform into amorphous phase[50] or more stable (and less porous) katsenite and dia polymorphs,[63,64] but the sodalite phase is still considered as the most interesting form for application and composite preparation.

We were inspired by the recent work by Brekalo et al.,[65] showing how the topology in imidazole-based ZIF ($Zn(im)_2$) can be directed even to thermodynamically unstable forms by templating with Me-$MeCH_2$ cavitand, in a process authors named the "shoe-last" principle. ZIF-8 was chosen as a host in our work due to the size, geometry, and hydrophobicity of the cavity that seemed particularly suitable for encapsulation and immobilization of C_{60} fullerene. It has large cages with a diameter of 11.6 Å, while the cage aperture is relatively small, only 3.4 Å in diameter.[57] Thus, with a diameter of ca. 6.8 Å,[66] C_{60} molecules can be comfortably accommodated in the ZIF-8 cavity. On the other hand, C_{60} should be efficiently immobilized as it is too large to pass through the cage aperture. We also expected that these small cage-apertures would prevent the preparation of C_{60}@ZIF-8 fulleretic materials from solution by soaking procedure unless the cage aperture is flexible and rearranges to allow the entering and transport of fullerene through the MOF structure.

Figure 1. Different concentration of C_{60} in mechanochemically-prepared C_{60}@ZIF-8. From left to right 0%, 30 %, 60 % and 100 % C_{60}@ZIF-8, respectively.

Synthesis of fulleretic C_{60}@ZIF-8 materials

ILAG of zinc oxide, 2-methylimidazole (2-MeIm), and defined amounts of fullerene, using ethanol and ammonium nitrate additives, resulted in rapid and tunable encapsulation of C_{60} in the ZIF-8 framework. The main idea was to avoid pushing the C_{60} molecules into the ZIF-8 cavities but rather to assemble the ZIF-8 framework around the fullerene template, without the need for dissolving the reactants, in particular fullerene. Partial encapsulation of C_{60} in ZIF-8 from an excess of fullerene was demonstrated recently in developing porous nitrogen-doped carbon anode for Li-ion batteries.[67] Herein, the loading of fullerene by ILAG was stoichiometry–controlled, and it required only traces of polar liquid additives as ethanol, in which the fullerene is insoluble, to facilitate the fulleretic formation. We designed the milling procedure in two steps. As it is well-established that the ball-milling is an excellent method for achieving a fast molecular diffusion in soft materials by breaking and recrystallizing the solid particles,[68] our initial step involved dry milling of ZnO, fullerene, and 2-methylimidazole in a ball-mill operating at 30 Hz, for 10-15 minutes, in order to mix the reactants thoroughly. PXRD analyses showed that no crystalline MOF was prepared at this stage (Figure S2a). In the second step, the milling was stopped for a short period, ethanol and ammonium nitrate additives were added to the milled reaction mixture, and milling was resumed for an additional 45 minutes. After the opening of the vessel, a dry purple microcrystalline powder was collected. This mechanochemical approach by ILAG required simple work-up by washing with a small volume of toluene. Even in higher target ratios, successful inclusion of fullerene guests could have been seen already during the washing. The products were sonicated during the washing procedure to remove the fullerene from ZIF-8 particles' surfaces, and even the initial wash-out was almost colorless (traces of fullerene color the toluene solution to intensive purple).

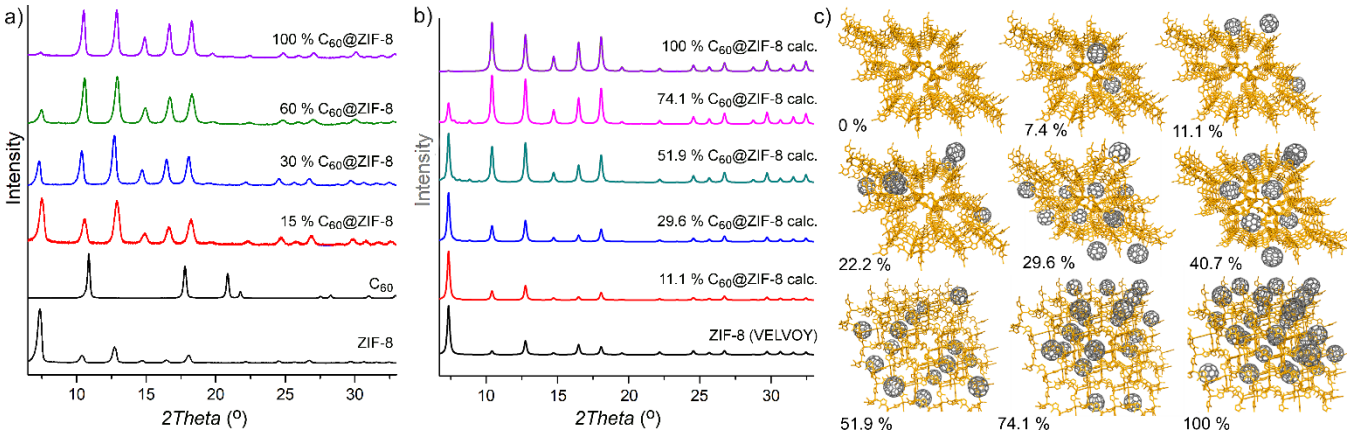

Figure 2. a) Experimental PXRD data for the mechanochemically prepared ZIF-8 and the C_{60}@ZIF-8 composites; b) Calculated PXRD data for ZIF-8 containing randomly oriented fullerenes placed in the randomly chosen voids of 3×3×3 unit cells; c) representation of randomly oriented fullerenes placed in the randomly chosen voids of 3×3×3 unit cell. Hydrogen atoms are omitted for clarity.

We have targeted four different C_{60}@ZIF-8 composites containing nominally 15 mol%, 30 mol%, 60 mol%, and 100 mol% of fullerene, relative to the maximum number of available cages in the structure of ZIF-8 (Cambridge Structural Database code VELVOY).[57] The purple color of C_{60}@ZIF-8 composites darkens with the increase in the fullerene content (Figure 1). One motivation for this work is developing a procedure for efficient encapsulation of rare and scarce endofullerenes, commonly available at sub-milligram levels. Thus, we also prepared C_{60}@ZIF-8 (30%) by capturing the sub-milligram amount of C_{60} (Figures S6 and S16). The EtOH and toluene filtrates are colorless, again proving the efficiency of the mechanochemical procedure (Figure S1). Guest-free ZIF-8 was prepared as a colorless microcrystalline solid in an identical ILAG procedure, only without adding the fullerene to the reaction mixture.

To test whether the C_{60} and 2-MeIm react in the first step, forming potentially specie that would not be encapsulated, we performed several milling experiments mimicking the procedure for the preparation of C_{60}@ZIF-8 composites, only without the addition of zinc source. The analyses of the resulting purple product show only the amorphization of the reaction mixture, and the milling products are soluble in our standard washing procedure (Figures S5 and S15).

Interestingly, milling of the pre-synthesized ZIF-8 with C_{60} fullerene resulted in a very low encapsulation despite the increased molecular mobility and particle recrystallization resulting from the ball-milling procedure.[68] Our results show that mechanochemical treatment on the formed ZIF-8 framework, where the cages may get disassembled and recrystallized by ball-milling to include the C_{60} template, resulted in very low loading, as evidenced from the color of the products and spectroscopic analysis. The products of the mechanochemical post-synthetic encapsulation attempts remained almost colorless after the washing, whereas the wash-outs were deep purple. It can be concluded that for the inclusion of the rigid and large guests as C_{60} fullerene into sodalite MOFs, the in situ mechanochemical formation of the framework around the C_{60} template is a much better approach.

We also attempted to prepare C_{60}@ZIF-8 from solution by post-synthetic soaking and in the solvothermal synthesis of the ZIF-8 in the presence of an excess of C_{60}, respectively. After a week of soaking of ZIF-8 in toluene containing an excess of fullerene, only a small amount of fullerene got encapsulated, which was evident from the sample's pale beige color and the PXRD and IR analyses (Figures S4 and S8). In situ solvothermal synthesis of ZIF-8 with fullerene in the DMF-toluene mixture at 120 °C also resulted in a low yield of C_{60}@ZIF-8 (Figure S4). The probable reason for such a low efficiency in encapsulation during solvothermal synthesis is the solvation and competition of the fullerene for the habitation of cages with the solvent molecules that are in vast excess, which is also suggested in spectroscopic analyses of fulleretic products (please see SI, section IR spectroscopy).

PXRD analysis

The absence of Bragg peaks characteristic for C_{60} confirms that ball milling yielded phase-pure C_{60}@ZIF-8 (Figure 2a), whereas the absence of Bragg peaks of ZnO reveals that the reaction was completed (Figure S2b). The encapsulation of C_{60} in ZIF-8 did not significantly influence the unit-cell parameters of the ZIF-8 structure; the position of the peaks is nearly identical to pure ZIF-8. Interestingly, the PXRD method can be used as a measure of the loading of fullerene in this MOF. The relative intensity of peaks in the PXRD of the composites changes with an increase in the fullerene content, which can be used to estimate the encapsulation extent. In more detail, the intensity of a low angle (110) peak of ZIF-8, at 2θ =7.3°, decreases[59,69–71] concurrently with the higher loading of C_{60}, whereas the intensity of (200) peak at 2θ =10.3° increases gradually until it becomes stronger than the (211) peak at 2θ =12.7° (Figure 2a). For the estimation of loading success, (110) peak is the most suitable to serve as a probe of the encapsulation success, as the changes in intensity are the most pronounced. A significant reduction of the intensity of the (110) mirror plane, which is positioned in the center of the cage, results from modified electronic density in the ZIF-8 cages due to the inclusion of hollow C_{60}. To rationalize and confirm this finding, we have built the ZIF-8 3×3×3 unit cell with different amounts of disordered fullerenes in the cages, using the atomic simulation environment (ASE) (Figure 2c).[72] The simulated PXRDs of such structures show excellent agreement with the experimentally observed PXRD data (Figure 2b), confirming that the reduction in the intensity of the (110) peak is indeed a direct result of the guest-inclusion. PXRD analysis also revealed a low degree of loading of fullerene in post-synthetic milling and solution strategies (Figures S3-S4).

IR spectroscopy

IR spectrum of C_{60}[73,74] is dominated by two bands at 577 and 528 cm^{-1}, ascribed to the radial motion of carbon atoms (Figure 3 and Figure S8). The other two bands, located at 1428 and 1182 cm^{-1}, are attributed to the tangential motion of carbon atoms, however this pair of bands is highly overlapped by ZIF-8 features (please

see SI, Figure S8) in IR spectra of samples obtained by encapsulation and confining of C_{60} inside the ZIF-8 cages. On the other hand, the radial-motion bands do not overlap with any bands of ZIF-8, so further in the text they serve as analytical markers. IR spectrum of the activated ZIF-8 is in excellent agreement with previous reports (Figure 3a and Figure S9).[57,75,76] The absorption bands for ZIF-8 at 3134 and 2929 cm^{-1} are due to the aromatic and aliphatic C–H stretch of imidazole, respectively. The band at 1583 cm^{-1} is attributed to C=N stretch. The bands in the region of 1500–1350 cm^{-1} are assigned to various stretching vibrations of the imidazole ring. The in-plane deformations of the ring dominate the 1350–900 cm^{-1} region, while those in the 800–650 cm^{-1} region are associated with the out-of-plane bending of the ring. The band at 420 cm^{-1} is ascribed to Zn–N stretch.

The 4000–2000 cm^{-1} region is not significantly affected by the encapsulation of C_{60} molecules inside the ZIF-8 framework. The changes are mostly located in the fingerprint region. At low C_{60} loadings (15% C_{60}@ZIF-8), the IR spectrum of ZIF-8 remains qualitatively more or less unaffected. However, higher loadings result in more noticeable spectral changes: (1) the envelope due to EtOH confined in the ZIF-8 cages, between 1280 and 1200 cm^{-1}, disappears and it is not present for 30% and higher loadings (Figure 3a and Figure S12); (2) ν(CC) and ν(CN) bands at 1425 and 1458 cm^{-1}, respectively (Figure S10), change their relative intensity. The most evident is the change in their intensity ratio with $x(C_{60})$. (3) the δ(NH)+ δ(CN) combination band at 1380 cm^{-1} suffers a significant increase in intensity, but it slowly decreases for $x(C_{60})$ over 30% (Figure S11) (4) 780-720 cm^{-1} envelope consists of two bands, one due to the out-of-plane imidazole ring deformations at 760 cm^{-1} and the other due to the in-plane ring deformation at 750 cm^{-1} (Figure S13). While the in-plane deformation band remains unaffected, the out-of-plane contribution significantly increases in intensity; (5) ν(ZnN) band shifts its position (Figure S14); (6 C_{60} bands due to radial motions are located at 525 and 576 cm^{-1}, respectively.

Intensities of both C_{60} bands follow the 2nd order polynomial function of $x(C_{60})$, qualitatively the same as observed for pure C_{60} in the KBr matrix. A comparison of the gas phase IR spectra of C_{60}[77] and previously considered UV/vis spectra indicates no significant interaction between the ZIF-8 framework and fullerene molecule, so we could consider the encapsulated C_{60} as almost free-standing inside the cage. This is corroborated by the Uv-vis measurements and molecular dynamics modeling discussed below.

The imidazole ring deformation bands change upon C_{60} encapsulation. This indicates that, although itself free-standing inside the cage, the encapsulated C_{60} molecule affects the dynamics of the imidazole linkers and the 3D MOF framework. This is in line with intuitive expectations since these constituents define the ZIF-8 cavity, which is now occupied by the bulk spherical C_{60}. The intensity of the δ(NH)+δ(CN) combination band at 1380 cm^{-1} initially significantly increases, but it slowly decreases for C_{60} loadings over 30% (Figure 3 and SI, Figure S11). DFTB-based MD modeling indicates that the transport of the fullerene molecules along the cages is hardly possible. To allow C_{60} to move to the next cage, all six imidazole rings of the aperture should exhibit concerted rotation. For ZIF-8, such a concerted change in the position of imidazoles is a low-probability event that may account for the low loading of C_{60} in the standard soaking approach. Far-IR spectroscopy of the ZIF-8[78] indicates the corresponding gate-opening mode at 33.4 cm^{-1}. Although this mode is far from the reach of available instrumentation, in- and out-of-plane imidazole ring deformation modes are indirectly informative in this respect. Namely, while the in-plane imidazole ring deformation band at 750 cm^{-1} remains unaffected by C_{60} loading, the out-of-plane contribution at 760 cm^{-1} significantly increases in intensity (Figure S13), in line with DFT findings obtained in this work at PBE/PAW level of theory (Figure 3b, and SI).

Additionally, both experiments and DFT clearly show intensification of the imidazole (CH_3)C–N stretching modes around 1460 cm^{-1}. All of these findings indicate the increased amplitude of out-of-plane movements of the imidazole rings.

As previously mentioned, the solvation and competition of the fullerene with solvent molecules is a possible reason for observed poor efficiency in C_{60} solvothermal encapsulation. The IR data revealed an interesting behavior of the broad 1280-1200 cm^{-1} envelope, which arises due to the EtOH confined inside the ZIF-8 cages, which completely disappears in fulleretic C_{60}@ZIF-8 materials with higher fullerene loading (Figure 3a and details in SI, section IR spectroscopy).

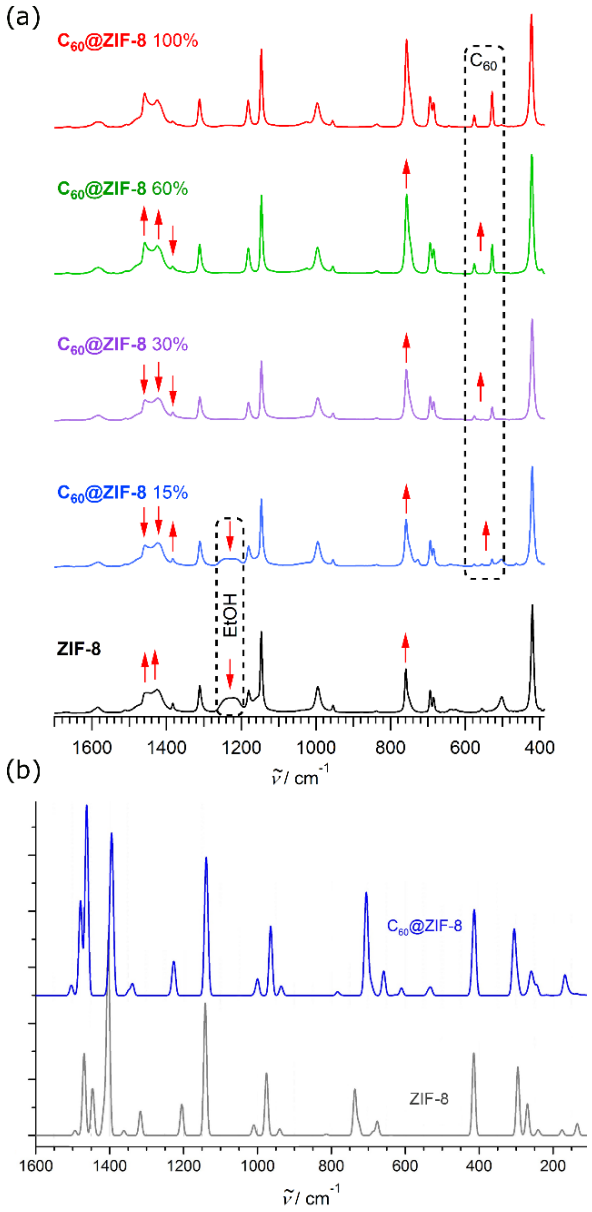

Figure 3. (a) Changes in the experimental IR spectra of ZIF-8 occurring due to the encapsulation of C_{60}. Features due to the dynamic relation of C_{60} and EtOH are framed by dashed rectangles. (b) DFT-computed IR spectra of C_{60}@ZIF-8 and empty ZIF-8.

The estimation of the C_{60} encapsulation efficiency was done by quantitative analysis of fullerene 528 and 577 cm^{-1} bands with respect to the standard crystalline C_{60} measured in the same conditions (Supporting Information, Section S4.2). Intensities (and other

spectral parameters) with respect to the C_{60} molar ratio are determined by fitting the 528 and 577 cm^{-1} bands, each band individually, to Lorentzian functions. For the 528 cm^{-1} band, fitting was done in the spectral range from 555 to 475 cm^{-1}, taking the ZIF-8 band at 504 cm^{-1} into consideration. Fitting of the 577 cm^{-1} band was done in the range from 610 to 550 cm^{-1}, taking the ZIF-8 band at 555 cm^{-1} into consideration. The corresponding bands for an equivalent amount of the C_{60} standards are considered in the same spectral ranges. The results are shown in Figure 4, while the details on the analysis are given in SI, Section S4.2. It can be concluded that C_{60} molecules are very efficiently encapsulated by the described mechanochemical strategy, reaching 95% efficiency at the highest loading. Post-synthetic loading by milling of fullerene and ZIF-8, and by soaking the ZIF-8 in toluene solution containing an excess of fullerene, resulted in low loading, 2.0 %, and 1.7 %, respectively (Figure 4), which is also evident from the color of the samples.

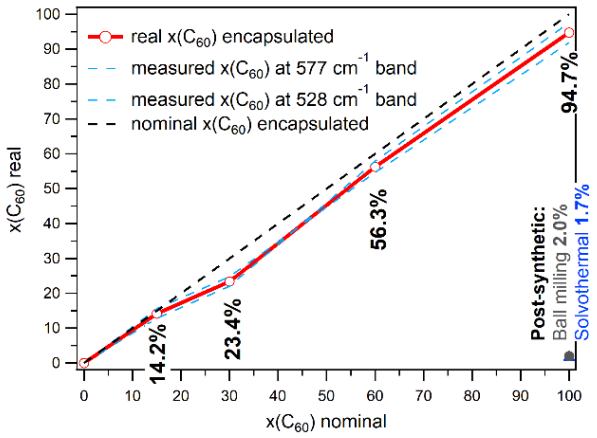

Figure 4. The efficiency of mechanochemical C_{60} encapsulation by ZIF-8. The post-synthetic loading attempts were done in excess of fullerene but resulted in low loading of ZIF-8 (black and blue points in the lower right corner).

UV-vis spectroscopy

UV-vis spectroscopic studies of C_{60}@ZIF-8 in the visible range were performed to understand how the encapsulation in ZIF-8 affects the electronic properties of C_{60}. Powder samples were placed onto KBr substrates and measured with an FT-IR microscope in the transmission mode; the solution is measured with a dispersive absorption spectrometer in a standard 1 cm quartz cell. Figure 5 compares the absorption spectra of the powder samples of ZIF-8, C_{60}, and C_{60}@ZIF-8. As expected for the colorless powder, ZIF-8 does not absorb light in the visible range and thus should not interfere with the light absorption by the encapsulated fullerene. C_{60}@ZIF-8 exhibits the onset of the absorption near 740 nm, followed by the band with well-resolved features at 622, 611, 600, and 591 nm. An absorption spectrum of C_{60} powder is substantially different from that of C_{60}@ZIF-8. The absorption onset of the fullerene powder is located at 780 nm and the absorption band at shorter wavelengths is broad and almost featureless except for the relatively sharp inflection at 685 nm. Thus, encapsulation in ZIF-8 shifts electronic transitions of C_{60} to higher energy and makes the features better resolved. These differences can be explained by the dramatically reduced interactions between C_{60} molecules in C_{60}@ZIF-8, resulting in nearly single-molecule properties. Indeed, a spectrum similar to C_{60}@ZIF-8 is obtained for C_{60} in diluted solutions (see Figure 5 for C_{60} in toluene and Ref. [79] for the spectrum in diluted hexane solution). Intermolecular interactions in crystalline C_{60} are comparably strong for the molecular crystal, leading to the significant dispersion of the HOMO- and LUMO-derived bands and, therefore, to the broadening of the absorption spectrum.

The differences of the electronic states of C_{60} in the ZIF-8 matrix and the fullerene powder are further corroborated by their luminescence spectra (Figure 5b). C_{60}@ZIF-8 shows the luminescence band with the maximum at 718 nm and several vibronic features, whereas the maximum of the solid C_{60} luminescence is shifted to 750 nm. Furthermore, we found that position of the peak in C_{60} powder depends on the sample morphology and excitation wavelength and shifts by 10-20 nm, whereas the spectrum of C_{60}@ZIF-8 is not affected by these measurement parameters or the load of C_{60} in ZIF-8. The fluorescence lifetime of C_{60}@ZIF-8 at room temperature is approximately 1.3 ns, and that of powder C_{60} is less than 1 ns. Thus, once again, we find that C_{60} entrapped in the ZIF-8 matrix shows different optical properties than the solid C_{60}. We can conclude that ZIF-8 appears to be a convenient matrix for the studies of almost "single-molecule" properties of fullerenes in the solid form without the need for substantial dilution.

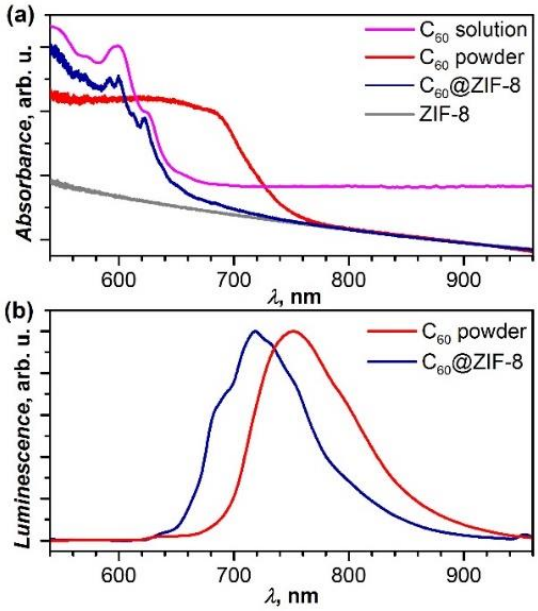

Figure 5. (a) Absorption spectra of ZIF-8, C_{60} powder, C_{60} solution in toluene, and C_{60}@ZIF-8 (100%) in the visible range. b) Luminescence spectra of C_{60}@ZIF-8 and C_{60} powder, excitation with the laser with λ = 515 nm.

ESR spectroscopy

The presence of fullerene guests in the cages of ZIF-8 is confirmed additionally by ESR spectroscopy. Off-the-shelf fullerene shows a weak sharp ESR line with g-value around g = 2.002 and peak-to-peak line-width around $W_{pp} \approx 0.1$ mT, due to defects in fullerene structure,[80–83] (Figure S21). While pristine ZIF-8 does not show this signal, both ESR investigated C_{60}@ZIF-8 (15%), and C_{60}@ZIF-8 (100%) exhibits a similar but broader $W_{pp} \approx 0.2$ mT fullerene line (Figure S21). ESR is a very sensitive technique, and the fact that the signal of encapsulated C_{60} remains similar to that of the crystalline fullerene reveals how mechanochemical treatment did not significantly damage the fullerene guests. Mechanochemistry looks like a reliable and suitable technique for fullerene loading. Importantly, no new paramagnetic defects were generated during the mechanochemical synthesis of C_{60}@ZIF-8 (Figure S22).

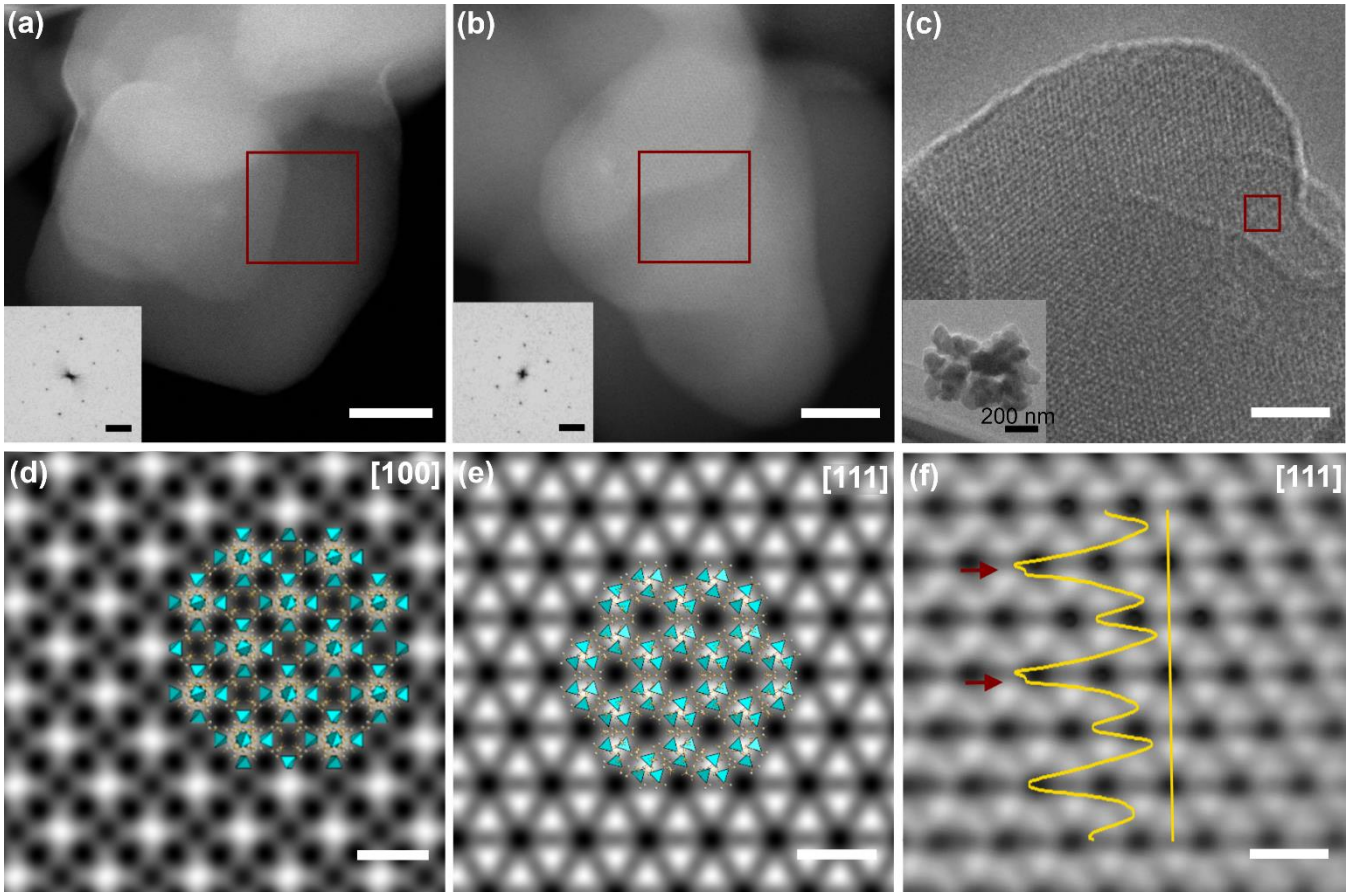

Figure 6. HAADF-STEM images of C_{60}@ZIF-8 along the [100] zone-axis (a), the [111] zone-axis (b). Insets show the fast Fourier transform (FFT) of the areas selected by red squares. (c) HRTEM image of C_{60}@ZIF-8 along the [111] zone-axis. The inset shows a typical low-resolution image of agglomerated particles. (d, e) Symmetry-imposed and lattice-averaged images along the [100] and [111] zone-axis, obtained using the CRISP software,[84] with a structural model of ZIF-8 embedded. Images d and e are cropped to 5×5 unit cells, and rotated by −125º and −61.3º, respectively, as compared to the areas outlined by red squares in images A and B. In HAADF-STEM, the contrast is approximately proportional to the square of the atomic number (Z); hence, the columns of the ZnN_4 tetrahedra (shown in cyan) are bright, and the voids are dark. (f) A zoomed region of the specimen is outlined by the red square in Figure 6c. The intensity profile along the yellow line shows some minor changes in the contrast close to the center of a ZIF-8 cage, not visible in Figure 6e. The scale bar for all images in the upper row is 15 nm, in the lower row – 2 nm.

HAADF-STEM and HRTEM analyses

MOF materials are known to be highly unstable under electron beam irradiation. To date, only a few studies have reported TEM imaging of MOFs, including MIL-101,[85] MOF-5,[86] UiO-66[87], and, very recently, ZIF-8.[88,89] C_{60}@ZIF-8 specimen was transferred to a lacey carbon grid by airflow. TEM experiments were carried out on a Themis Z (Thermo Fisher Scientific) microscope operated at 300 kV. We tested the C_{60}@ZIF-8 specimen at the liquid nitrogen temperature following the procedure by Li et al.[88]; however, no improvement in the resolution was gained, therefore the structure characterization described below has been conducted at non-cryogenic conditions.

The crystals of C_{60}@ZIF-8 (100%) obtained by ball milling are typically ∼70 ± 15 nm in size, non-uniformly shaped, and tend to agglomerate. Crystals with a square cross-section and 90° angles between the surface facets commonly lie on the carbon support in the [100] zone-axis orientation (Figure 6a), and those having a triangular shape are close to the [111] zone-axis (Figure 6b). Although MOFs are often vulnerable under scanning transmission electron microscopy (STEM) conditions, it was possible to collect the images shown in Figure 6a and b using the high-angle annular dark-field scanning transmission electron microscopy, HAADF-STEM, settings, and achieve a high resolution. It is worth noting that the pristine ZIF-8 immediately loses its crystallinity under STEM conditions while being illuminated with the same electron dose as C_{60}@ZIF-8. While the fullerene loading did little to affect the thermal stability of the composites (SI, Section S8), it leads to improved beam stability. This increase in stability can be considered as additional indirect evidence of filling the cages in the ZIF-8 structure and a particularly exciting feature of the C_{60}@ZIF-8 composites. The lattice parameter a = 17.1 Å, obtained from the fast Fourier transform (FFT) (insets in Figures 6a and 6b), is in agreement with the value reported for the pristine ZIF-8 in the literature (a = 17.03 Å, [CSD code VELVOY])[57] and the experimental PXRD data (Figure 2a). The d-spacings up to 5.5 Å are resolvable from the FFT. Therefore the individual ZnN_4 tetrahedra located at ∼3.4 Å apart from each other cannot be distinguished. Imposing a projection symmetry (*P*31*m* and *P*4*m*, correspondingly) on the lattice-averaged images results in a good match to the structural model of ZIF-8 along with both the [111] and [100] directions, thus providing additional proof that the ZIF-8 framework is retained during the C_{60}@ZIF-8 preparation by ball milling (Figures 6d and 6e). Since the contrast in HAADF-STEM is predominantly formed by the Zn metal centers (Figures 6a and 6b), we also took a high-resolution TEM (HRTEM) image of the C_{60}@ZIF-8 viewed along the [111] zone axis (Figure 6c). The image has been both Fourier filtered and bandpass filtered in order to reduce random noise. At

the given value of defocus, the HRTEM image has an inverted contrast: dark regions correspond to the cage space, whereas bright areas are formed by the Zn metal centers. The HRTEM image has additional features which have not been revealed and confirmed by HAADF-STEM experiments. Namely, for some thin areas of the specimen, an additional contrast was found approximately in the center of the ZIF-8 main channels, corresponding to the most energetically favorable position of the C_{60} molecule in the ZIF-8 framework, according to the calculated energy profile shown in Figure 7. Such a feature has been already reported as TEM evidence of CO_2 loading in ZIF-8.[88] Here, based on the collected TEM data alone, this contrast cannot be unambiguously attributed to the real fullerene position in the structure. However, this finding lays a path towards further investigations of the electron-dose-stable ZIF-8 composites and their local structure on the atomic level.

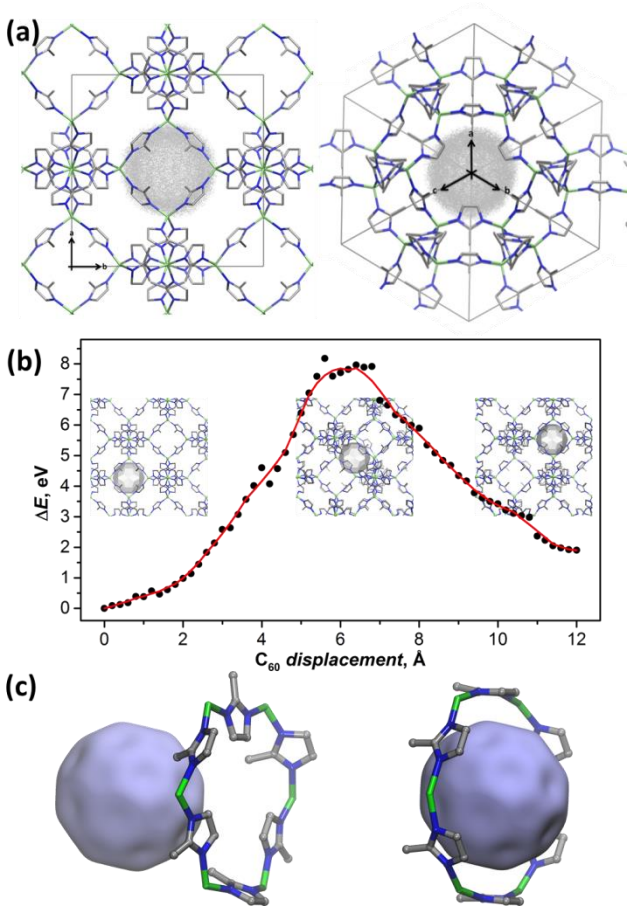

Figure 7. (a) DFTB-based molecular dynamics simulations of C_{60}@ZIF-8 at 300 K (left and right parts visualize two orientations of the structure). Grey dots show all positions of carbon atoms in the 250 ps trajectory. (b) DFTB-based energy profile and selected configuration of C_{60}@ZIF-8 obtained while dragging the C_{60} molecule from one cage to the neighboring cage through the larger aperture. (c) The structure of the aperture with two positions of C_{60}: in the middle of the cage (left) and in the moment of passing through the aperture (right). Hydrogen atoms and the rest of the ZIF-8 structure are omitted for clarity.

Molecular dynamics simulations

To get further insight into the location and dynamics of C_{60} molecules inside ZIF-8, molecular dynamics simulations were performed using a density-functional based tight-binding method (DFTB). The calculations showed that C_{60} could freely rotate and oscillate near the center of the cage. However, over the whole 250 ps trajectory with a Nosé-Hoover thermostat temperature of T = 300 K, we did not observe a single event of passing from one cage to another (Figure 7a and SI), indicating that the C_{60} migration through ZIF-8, if possible at all, must be very rare. Once C_{60} is encapsulated into a cage, it is likely to remain in that position. This contrasts with previous studies of the successful inclusion of small gases (N_2, CO_2) into empty ZIF-8. The previous reports talk about the "gate-opening" phenomenon in a relatively flexible structure of ZIF-8.[90,91,92] The methyl groups of 2-methylimidazole linkers spatially rearrange, ensuring the capture of gases bigger than the aperture.

Since the observation of a spontaneous movement of fullerene between the cages is not feasible on a reasonable timescale, the C_{60} molecule was dragged from one cage to another using distance constrain between a carbon atom in the fullerene cage and the center of the targeted cage. In contrast, all other degrees of freedom were allowed to relax. Figure 7b shows the energy profile obtained in the course of such a trajectory (please see SI for computational details and the full propagation path animation). The calculation reveals that the migration of C_{60} between the cages requires overcoming a substantial barrier of ca 8 eV. Although the reliability of the DFTB approach in the precise estimation of the relative energies for this system is probably not very high, the prohibitively large barrier is another confirmation of the low loading efficiency in a solution soaking process or post-synthetic mechanochemical loading. The primary reason for a large energy demand can be well seen in Figure 7c, which compares the geometry of the aperture for two positions of the fullerene molecule, one in the center of the cage and another one at the moment when C_{60} passes through the orifice. To let C_{60} pass through, all methylimidazole units should orient in a concerted manner parallel to the C_{60} surface, and the ring should expand by a considerable rearrangement of all N–Zn–N angles.

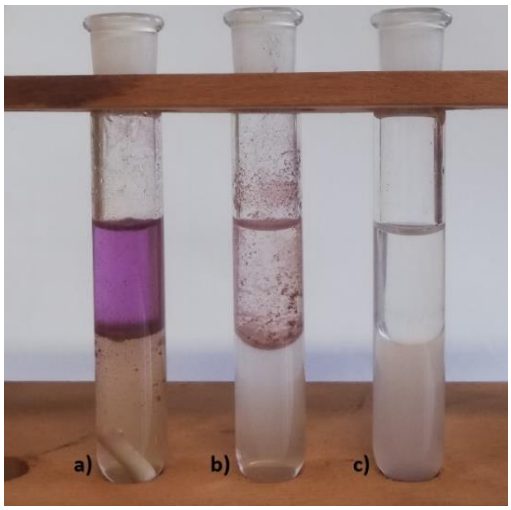

Figure 8. Test tubes with C_{60}@ZIF-8 added to layered H_2O and toluene after the addition of a) 0.5 mol dm^{-3} HCl (aq), and b) 1 mol dm^{-3} KOH (aq). For c) C_{60}@ZIF-8 was initially dispersed in a basic solution of 1 mol dm^{-3} KOH (aq), and toluene was added subsequently. The releasing was only observed in a).

pH-controlled releasing of C_{60}

The releasing experiments also prove that C_{60} is effectively captured and immobilized in the sodalite framework. The fulleretics remain stable in neutral or basic solutions (water/toluene mixtures) and do not release C_{60} upon sonication. However, C_{60} gets released almost immediately under acidic conditions (pH 2-4) (Figure 8),

revealing that the releasing process can be controlled by the acidity of the environment, which one has to bear in mind in potential applications of C_{60}@ZIF-8 fulleretics. The sensitivity of ZIFs to the acidic environment is well-studied,[93] and it is already used for the pH-controlled release of encapsulated drug molecules from MOF vehicles, such as for example 5-fluorouracil@ZIF-8.[94] Slow release of the 5-fluorouracil from the ZIF-8 voids can be dramatically accelerated by lowering the pH of the slurry from 7.4 to 5.0, following the difference between the normal blood pH and the pH of cancer cells. The release of 5-fluorouracil was followed by the dissolution of the ZIF-8 structure, a degradation of the framework, and the rise of Zn^{2+} ions in the solution.[93,95]

CONCLUSIONS

To summarize, we have shown here how the mechanochemical ILAG approach leads to rapid, efficient, green, and controllable preparation of four tunable fulleretic materials, with specified amounts of C_{60}-fullerene guests. This mechanochemical strategy, involving cheap and easily accessible reactants such as ZnO and ethanol, proved superior to the solution synthetic and post-synthetic procedures. It avoided problems related to solubility, solvation, the competition of the target fullerene with the solvent molecules, and small cage-apertures. It allowed for a high level of stoichiometrically-controlled loading of the buckminsterfullerene into the cages of ZIF-8. The confinement of C_{60} in the ZIF-8 cage does not influence the unit-cell parameters of ZIF-8, but increases the rigidity of the framework and improves the stability of fulleretic material towards the electron dose radiation. While the HAADF-STEM could not provide unambiguous proof on the fullerene's exact position in the cages, the DFTB-based molecular dynamics studies indicate that the hollow fullerene is accommodated in the middle of the cage, which also rationalizes the changes in the IR and PXRD data observed upon encapsulation. Once entrapped, the fullerene is immobilized in one cage, and the transport of the fullerene through the network requires energy and substantial rearrangement in the aperture structure. The entrapped C_{60} molecules are in a weak interaction with the MOF wall and well isolated one from the other, even in high loading. This makes ZIF-8 a convenient matrix for the efficient immobilization of fullerene guests and achieving well ordered, almost "single-molecule" properties of fullerenes in the solid form without substantial dilution. Due to the high-efficiency of the presented mechanochemical procedure, we aim to apply this mechanochemical strategy for entrapment of anisotropic and magnetic metallofullerenes available at sub-milligram scale, to develop fulleretic materials with tunable content of magnetic centers, and to expand the interesting but poorly investigated field of fulleretic materials. We believe this strategy may prove general also for the stoichiometry-controlled confinement of other rigid nano-guests, such as polyoxometalates or metallic nanoparticles in MOF(s) with suitable structure and nature of the voids.

EXPERIMENTAL

Materials. ZnO, ammonium nitrate, and 2-methyl imidazole (MeIm) were obtained from Sigma-Aldrich. Ethanol (EtOH) was purchased from Grammol. Toluene was obtained from Sigma Aldrich. Fullerene-C_{60} was supplied from TCI.

Mechanochemical synthesis of ZIF-8. ZIF-8 was synthesized according to the literature method.[49]

Mechanochemical syntheses of C_{60}@ZIF-8 materials. ZnO (40 mg, 0.491 mmol), 2-methyl imidazole (80.70 mg, 0.982 mmol) and C_{60} (9 mg (15 %)) were placed into a Teflon jar with two stainless steel balls (7 mm). The mixture was neatly ground for 10 min at 30 Hz using IST-500 mixer mill followed by addition of EtOH (45 μL) and 6 mg of NH_4NO_3 for 45 min further milling. The resulting compound was washed first with EtOH then toluene, filtered and air dried. Purple compound was obtained and analyzed by PXRD, FTIR-ATR and TGA. The quantity of C_{60} was calculated on the basis of the maximum number of voids in ZIF-8 structure which accounts for 1/6 of the ZIF-8 total quantity. The reaction has been repeated using different ratio of C_{60} (18 mg, (30%), 36 mg (60%), 60 mg (100 %). Elemental analysis calculated (%) for ZIF-8 ($C_8H_{10}N_4Zn$); C:42.22, H: 4.43, N:24.62, found C:43.40, H: 5.11, N: 21.32. For 30 % C_{60}@ZIF-8 ($C_{11}H_{10}N_4Zn$); C:50.11, H: 3.82, N:21.25, found C:49.00, H: 4.31, N: 19.82. For 100% C_{60}@ZIF-8 ($C_{18}H_{10}N_4Zn$); C:62.18, H: 2.90, N:16.11, found C:59.31, H: 3.88, N: 16.16.

Small-scale mechanochemical synthesis of 30% C_{60}@ZIF-8 material. ZnO (2 mg, 0.0245 mmol), 2-methyl imidazole (4 mg, 0.0491 mmol) and C_{60} (0.9 mg (30 %)) were placed into a Teflon jar with two stainless steel balls (7 mm). The mixture was neatly ground for 10 min at 30 Hz using IST-500 mixer mill followed by the addition of EtOH (5 μL) and 0.4 mg of NH_4NO_3 for 45 min further milling. The resulting compound was washed first with EtOH then toluene, following the procedure stated above, filtered, and air-dried. Purple compound was obtained and analyzed by PXRD and FTIR-ATR.

Neat grinding of 2-methyl imidazole and C_{60}. 2-methyl imidazole (25 mg, 0.306 mmol) and C_{60} (12,5 mg) were placed into a Teflon jar with two stainless steel balls (7 mm). The mixture was neatly ground for 1 hour at 30 Hz using IST-500 mixer mill. The resulting product was analyzed by PXRD and FTIR-ATR. The milling product dissolves by washing with EtOH and toluene following procedure stated above.

ILAG of 2-methyl imidazole and C_{60}. 2-methyl imidazole (25 mg, 0.306 mmol) and C_{60} (12,5 mg) were placed into a Teflon jar with two stainless steel balls (7 mm). The mixture was neatly ground for 15 minutes at 30 Hz using IST-500 mixer mill followed by further milling by the addition of NH_4NO_3 (3 mg) and 20 μL of EtOH. The resulting crude product was analyzed by PXRD and FTIR-ATR. The milling product was dissolved by washing with EtOH and toluene, following procedure stated above.

ILAG of 2-methyl imidazole. 2-methyl imidazole (25 mg, 0.306 mmol) and NH_4NO_3 (3 mg) were placed into a Teflon jar with two stainless steel balls (7 mm). EtOH (20 μL) was added and the mixture was milled for 30 minutes. The resulting product was analyzed by PXRD and FTIR-ATR.

Post-synthetic method for the encapsulation of C_{60} into mechanochemically-synthesized ZIF-8. 15 mg mechanochemically-synthesized ZIF-8 and 15 mg fullerene-C_{60} were placed into a Teflon jar with two stainless steel balls (7 mm). The mixture was milled for 45 minutes at 30 Hz using IST-500 mixer mill. Resulting powder was washed with toluene three times (3×10 mL). Beige-colored solid was analyzed by PXRD and FTIR-ATR.

Solvothermal synthesis of ZIF-8 and post-synthetic encapsulation of C_{60} by soaking in toluene solution. $Zn(NO_3)_2{\cdot}6H_2O$ (108.70 mg, 0.365 mmol) and 2-methyl imidazole (60 mg, 0.730 mmol) were each dissolved in 5 mL of DMF. Prepared solutions were placed into a 20 mL Teflon-lined stainless steel autoclave. The mixture was then heated for 24 hours at 120°C. A white powder was precipitated and washed with DMF, air-dried and analyzed by PXRD and FTIR-ATR. Resulting solid was then soaked for a week in toluene solution with excess amount of C_{60} fullerene. Beige-colored solid was analyzed by PXRD and FTIR-ATR.

One-pot solvothermal synthesis of C_{60}@ZIF-8 materials. $Zn(NO_3)_2{\cdot}6H_2O$ (108.70 mg, 0.365mmol) and 2-methyl imidazole (60 mg, 0.730 mmol) were each dissolved in 5 mL of DMF. Prepared solutions and 8 mL of toluene solution of C_{60} (25 mg, 0.0346 mmol) were placed into a 20 mL Teflon-lined stainless steel autoclave. The mixture was then autoclaved for 24 hours at 120°C. Obtained precipitate was light colored while mother liquid stayed purple. It was subsequently washed several times with DMF and then with toluene. Beige colored solid was analyzed by PXRD and FTIR-ATR.

Activation of C_{60}@ZIF-8 samples for IR measurements. C_{60}@ZIF-8 samples were washed with EtOH three times and soaked in EtOH for two days by changing EtOH three times in a day. Afterwards, they were left under 100°C overnight.

Releasing experiments

TEST TUBE 1: 5 mg suspension of C_{60}@ZIF-8 in deionized H_2O (5mL) was stirred at RT, while 0.5 mol dm^{-3} HCl (aq) was added dropwise and resulting mixture was ultra-sounded for a few seconds. By the color of the suspension started to turn to brown, toluene was added to the mixture. Toluene phase turned to purple immediately, what is the evidence of successful release of fullerene C_{60}.

TEST TUBE 2: 5 mg C_{60}@ZIF-8 was added to the mixed layer of deionized H_2O (5 mL) and toluene (5 mL) and stirred at RT, while 1 mol dm^{-3}

KOH (aq) was added dropwise. Resulting mixture was ultra-sounded for a few seconds. No color change was observed, since C_{60} was unable to be released from the pores.

TEST TUBE 3: 5 mg suspension of C_{60}@ZIF-8 in deionized H_2O (5 mL) was stirred at RT, while 1 mol dm^{-3} KOH (aq) was added dropwise and resulting mixture was ultra-sounded for a few seconds. By the color of the suspension started to turn to brown, toluene was added to the result mixture. No color change was observed, since C_{60} was unable to be released from the pores.

Powder X-ray diffraction (PXRD). PXRD data for as-synthesized samples was analyzed by PanalyticalAeris Research tabletop diffractometer, with CuK_α radiation (40 kV, 7.5 mA) in Bragg Bretano geometry, with the sample mounted on zero background silicon plate.

FTIR spectroscopy. Measurements were performed on a PerkinElmer Fourier transform infrared spectrometer Spectrum Two (PerkinElmer,Inc.) using Spectrum10 software (PerkinElmer, Inc.) in transmittance mode by KBr pellet technique and FTIR-ATR.

Vis-NIR absorption spectroscopy. Absorption spectra of ZIF-8, C_{60}, and C_{60}@ZIF-8 powder samples in the visible range were measured with Hyperion microscope attached to Vertex FTIR spectrometer (Bruker). Powder samples were placed onto KBr single-crystal substrates and the spectra were measured in transmission mode. Absorption spectrum of the fullerene solution in toluene was measured with dispersive UV-vis-NIR spectrometer Shimadzu UV 3101PC.

Luminescence spectroscopy. Steady-state luminescence spectra of powder samples were measured with a modular spectrometer of local design comprising Omicron PhoxX diode lasers for excitation (405 nm, 488 nm, 515 nm), Avantes AvaSpec HS1024x122TEC high-sensitivity fiber-optic spectrometer with TE-cooled backthinned CCD detector (200–1000 nm), and optical microscope of local design. Variable-temperature measurements were performed with Janis ST-500 microscopy cryostat (temperatures down to 4 K). Luminescence lifetimes were measured by time-correlated single photon counting (TCSPC) technique using PicoQuant TimeHarp counter/timer and the FluoFit software. Luminescence is excited by Omicron diode lasers modulated up to the frequency of 80 MHz (allowing the measurement of lifetimes longer than ~0.7 ns), time-resolved detection is performed by a PMA 192 PMT (Picoquant) in a visible range (250-850 nm).

ESR spectroscopy. The electron spin resonance (ESR) or electron paramagnetic resonance (EPR) study was performed on powder samples in the range from room temperature down to 78 K using a Bruker Elexsys 580 FT/CW X-band spectrometer. Microwave frequency was around 9.7 GHz, magnetic field modulation amplitude was 0.03 mT and modulation frequency was 100 kHz.

TGA experiments. All TGA experiments were performed by simultaneous thermal analyzer STA 6000 (PerkinElmer, Inc.) in alumina crucibles at 5°C min^{-1} heating rate from 35°C to 900°C under nitrogen gas, and from 35°C to 800°C under oxygen gas, respectively, purging at flow of 30 mL min^{-1}.

ASSOCIATED CONTENT

Supporting Information

The Supporting Information is available free of charge on the ACS Publications website. Description of methods, PXRD, IR, and TGA data, and the animation of the transport of fullerene through the ZIF-8 structure.

AUTHOR INFORMATION

Corresponding Author

*E-mail: A.Popov@ifw-dresden.de, krunoslav.uzarevic@irb.hr

Present Addresses

† Division of Physical Chemistry, Ruđer Bošković Institute, HR-10000, Zagreb, Croatia

Notes

The authors declare no competing financial interests.
¥ These authors contributed equally.

ACKNOWLEDGMENT

We thank Prof. M. Ilakovac Kveder for the discussions. M.R. cordially thanks Tom Willhammar and Xiaodong Zou for the helpful discussion and acknowledges the financial support of the Knut and Alice Wallenberg Foundation for the CATSS project (KAW 2016.0072). Frank Ziegs and Sandra Schiemenz are acknowledged for help with spectroscopic measurements in IFW Dresden. The authors acknowledge the Croatian Science Foundation (grant no. IP-2018-01-3168) and German (DAAD)-Croatian (MZO) bilateral project: *Magneto-structural correlations in molecular magnetic complexes studied by electron spin resonance spectroscopy* for financial support. The work has been supported in part by the "Research Cooperability "Program of the Croatian Science Foundation funded by the European Union from the European Social Fund under the Operational Programme Efficient Human Resources 2014-2020, through grant PZS-2019-02-4129. IL acknowledges support from the European Union through the European Regional Development Fund within the Competitiveness and Cohesion Operational Programme (Grant No.~KK.01.1.1.06). AAP thanks Deutsche Forschungsgemeinschaft for financial support (projects PO 1602/4-1 and 1602/6-1).

REFERENCES

(1) Ortiz, Michael; Cho, Sung; Niklas, Jens; Kim, Seonah; Poluektov, Oleg G.; Zhang, Wei; Rumbles, Garry; Park, Jaehong. Through-Space Ultrafast Photoinduced Electron Transfer Dynamics of a C 70 -Encapsulated Bisporphyrin Covalent Organic Polyhedron in a Low-Dielectric Medium. *J. Am. Chem. Soc.* **2017**, *139* (12), 4286–4289. https://doi.org/10.1021/jacs.7b00220.

(2) Guldi, Dirk M.; Illescas, Beatriz M.; Atienza, Carmen M[a]; Wielopolski, Mateusz; Martín, Nazario. Fullerene for Organic Electronics. *Chem. Soc. Rev.* **2009**, *38* (6), 1587. https://doi.org/10.1039/b900402p.

(3) Jeon, Il; Ueno, Hiroshi; Seo, Seungju; Aitola, Kerttu; Nishikubo, Ryosuke; Saeki, Akinori; Okada, Hiroshi; Boschloo, Gerrit; Maruyama, Shigeo; Matsuo, Yutaka. Lithium-Ion Endohedral Fullerene (Li + @C 60) Dopants in Stable Perovskite Solar Cells Induce Instant Doping and Anti-Oxidation. *Angew. Chemie Int. Ed.* **2018**, *57* (17), 4607–4611. https://doi.org/10.1002/anie.201800816.

(4) Ghiassi, Kamran B.; Olmstead, Marilyn M.; Balch, Alan L. Gadolinium-Containing Endohedral Fullerenes: Structures and Function as Magnetic Resonance Imaging (MRI) Agents. *Dalt. Trans.* **2014**, *43* (20), 7346–7358. https://doi.org/10.1039/C3DT53517G.

(5) Chen, Chia-Hsiang; Krylov, Denis S.; Avdoshenko, Stanislav M.; Liu, Fupin; Spree, Lukas; Yadav, Ravi; Alvertis, Antonis; Hozoi, Liviu; Nenkov, Konstantin; Kostanyan, Aram; et al. Selective Arc-Discharge Synthesis of Dy 2 S-Clusterfullerenes and Their Isomer-Dependent Single Molecule Magnetism. *Chem. Sci.* **2017**, *8* (9), 6451–6465. https://doi.org/10.1039/C7SC02395B.

(6) Liu, Fupin; Wang, Song; Gao, Cong-Li; Deng, Qingming; Zhu, Xianjun; Kostanyan, Aram; Westerström, Rasmus; Jin, Fei; Xie, Su-Yuan; Popov, Alexey A.; et al. Mononuclear Clusterfullerene Single-Molecule Magnet Containing Strained Fused-Pentagons Stabilized by a Nearly Linear Metal Cyanide Cluster. *Angew. Chemie Int. Ed.* **2017**, *56* (7), 1830–1834. https://doi.org/10.1002/anie.201611345.

(7) Liu, Ying; Chen, Chunying; Qian, Pengxu; Lu, Xuefei; Sun, Baoyun; Zhang, Xiao; Wang, Liming; Gao, Xingfa; Li, Han; Chen, Zhiyun; et al. Gd-Metallofullerenol Nanomaterial as Non-Toxic Breast Cancer Stem Cell-Specific Inhibitor. *Nat. Commun.* **2015**, *6* (1), 5988. https://doi.org/10.1038/ncomms6988.

(8) Zheng, Deng-Yue; Chen, En-Xuan; Ye, Chun-Rong; Huang, Xiao-Chun. High-Efficiency Photo-Oxidation of Thioethers over C 60 @PCN-222 under Air. *J. Mater. Chem. A* **2019**, *7* (38), 22084–22091. https://doi.org/10.1039/C9TA07965C.

(9) Gao, Yi; Wu, Xiaojun; Zeng, Xiao Cheng. Designs of Fullerene-Based Frameworks for Hydrogen Storage. *J. Mater. Chem. A* **2014**, *2* (16), 5910–5914. https://doi.org/10.1039/C3TA13426A.

(10) Popov, Alexey A.; Yang, Shangfeng; Dunsch, Lothar. Endohedral Fullerenes. *Chem. Rev.* **2013**, *113* (8), 5989–6113. https://doi.org/10.1021/cr300297r.

(11) Jin, Peng; Li, Ying; Magagula, Saneliswa; Chen, Zhongfang. Exohedral Functionalization of Endohedral Metallofullerenes: Interplay between inside and Outside. *Coord. Chem. Rev.* **2019**, *388*, 406–439. https://doi.org/10.1016/j.ccr.2019.02.028.

(12) Rice, Allison M.; Dolgopolova, Ekaterina A.; Shustova, Natalia B. Fulleretic Materials: Buckyball- and Buckybowl-Based Crystalline Frameworks. *Chem. Mater.* **2017**, *29* (17), 7054–7061. https://doi.org/10.1021/acs.chemmater.7b02245.

(13) Williams, Derek E.; Dolgopolova, Ekaterina A.; Godfrey, Danielle C.; Ermolaeva, Evgeniya D.; Pellechia, Perry J.; Greytak, Andrew B.; Smith, Mark D.; Avdoshenko, Stanislav M.; Popov, Alexey A.; Shustova, Natalia B. Fulleretic Well-Defined Scaffolds: Donor–Fullerene Alignment Through Metal Coordination and Its Effect on Photophysics. *Angew. Chemie Int. Ed.* **2016**, *55* (31), 9070–9074. https://doi.org/10.1002/anie.201603584.

(14) Chae, Hee K.; Siberio-Pérez, Diana Y.; Kim, Jaheon; Go, YongBok; Eddaoudi, Mohamed; Matzger, Adam J.; O'Keeffe, Michael; Yaghi, Omar M. A Route to High Surface Area, Porosity and Inclusion of Large Molecules in Crystals. *Nature* **2004**, *427* (6974), 523–527. https://doi.org/10.1038/nature02311.

(15) Matsuzaki, Shohei; Arai, Tatsuhiko; Ikemoto, Koki; Inokuma, Yasuhide; Fujita, Makoto. Networked-Cage Microcrystals for Evaluation of Host–Guest Interactions. *J. Am. Chem. Soc.* **2014**, *136* (52), 17899–17901. https://doi.org/10.1021/ja5109535.

(16) Brenner, Wolfgang; Ronson, Tanya K.; Nitschke, Jonathan R. Separation and Selective Formation of Fullerene Adducts within an M II 8 L 6 Cage. *J. Am. Chem. Soc.* **2017**, *139* (1), 75–78. https://doi.org/10.1021/jacs.6b11523.

(17) Meng, Haibing; Wang, Chunru; Wang, Taishan; Meng, Haibing; Wang, Chunru; Wang, Taishan. Molecular Fullerenes Encapsulated in Metal-Organic Frameworks. *Gen. Chem.* **2018**, *4* (4), 180019. https://doi.org/10.21127/yaoyigc20180019.

(18) Cirujano, F. G.; Llabrés i Xamena, F. X. Metal Organic Frameworks as Nanoreactors and Host Matrices for Encapsulation. In *Organic Nanoreactors*; Sadjadi, Samahe B. T. Organic Nanoreactors, Ed.; Elsevier: Boston, 2016; pp 305–340. https://doi.org/10.1016/B978-0-12-801713-5.00010-0.

(19) Meng, Haibing; Zhao, Chong; Nie, Mingzhe; Wang, Chunru; Wang, Taishan. Changing the Hydrophobic MOF Pores through Encapsulating Fullerene C 60 and Metallofullerene Sc 3 C 2 @C 80. *J. Phys. Chem. C* **2019**, *123* (10), 6265–6269. https://doi.org/10.1021/acs.jpcc.8b11659.

(20) Krylov, D. S.; Liu, F.; Brandenburg, A.; Spree, L.; Bon, V.; Kaskel, S.; Wolter, A. U. B.; Büchner, B.; Avdoshenko, S. M.; Popov, A. A. Magnetization Relaxation in the Single-Ion Magnet DySc 2 N@C 80 : Quantum Tunneling, Magnetic Dilution, and Unconventional Temperature Dependence. *Phys. Chem. Chem. Phys.* **2018**, *20* (17), 11656–11672. https://doi.org/10.1039/C8CP01608A.

(21) Goswami, Subhadip; Ray, Debmalya; Otake, Ken-ichi; Kung, Chung-Wei; Garibay, Sergio J.; Islamoglu, Timur; Atilgan, Ahmet; Cui, Yuexing; Cramer, Christopher J.; Farha, Omar K.; et al. A Porous, Electrically Conductive Hexa-Zirconium(<scp>iv</Scp>) Metal–Organic Framework. *Chem. Sci.* **2018**, *9* (19), 4477–4482. https://doi.org/10.1039/C8SC00961A.

(22) García-Simón, Cristina; Costas, Miquel; Ribas, Xavi. Metallosupramolecular Receptors for Fullerene Binding and Release. *Chem. Soc. Rev.* **2016**, *45* (1), 40–62. https://doi.org/10.1039/C5CS00315F.

(23) Inokuma, Yasuhide; Arai, Tatsuhiko; Fujita, Makoto. Networked Molecular Cages as Crystalline Sponges for Fullerenes and Other Guests. *Nat. Chem.* **2010**, *2* (9), 780–783. https://doi.org/10.1038/nchem.742.

(24) Zheng, Deng-Yue; Zhou, Xue-Meng; Mutyala, Suresh; Huang, Xiao-Chun. High Catalytic Activity of C 60 Pd n Encapsulated in Metal–Organic Framework UiO-67, for Tandem Hydrogenation Reaction. *Chem. – A Eur. J.* **2018**, *24* (72), 19141–19145. https://doi.org/10.1002/chem.201803900.

(25) Li, Haiqing; Hill, Matthew R.; Huang, Runhong; Doblin, Christian; Lim, Seng; Hill, Anita J.; Babarao, Ravichandar; Falcaro, Paolo. Facile Stabilization of Cyclodextrin Metal–Organic Frameworks under Aqueous Conditions via the Incorporation of C 60 in Their Matrices. *Chem. Commun.* **2016**, *52* (35), 5973–5976. https://doi.org/10.1039/C6CC01620K.

(26) Pratik, Saied Md; Gagliardi, Laura; Cramer, Christopher J. Boosting Photoelectric Conductivity in Porphyrin-Based MOFs Incorporating C 60. *J. Phys. Chem. C* **2020**, *124* (3), 1878–1887. https://doi.org/10.1021/acs.jpcc.9b10834.

(27) Feng, Yong-qiang; Wang, Taishan; Li, Yongjian; Li, Jie; Wu, Jingyi; Wu, Bo; Jiang, Li; Wang, Chunru. Steering Metallofullerene Electron Spin in Porous Metal-Organic Framework. *J. Am. Chem. Soc.* **2015**, *137*. https://doi.org/10.1021/jacs.5b10796.

(28) Avdoshenko, Stanislav M.; Fritz, Fabian; Schlesier, Christin; Kostanyan, Aram; Dreiser, Jan; Luysberg, Martina; Popov, Alexey A.; Meyer, Carola; Westerström, Rasmus. Partial Magnetic Ordering in One-Dimensional Arrays of Endofullerene Single-Molecule Magnet Peapods. *Nanoscale* **2018**, *10* (38), 18153–18160. https://doi.org/10.1039/C8NR05386C.

(29) Meng, Haibing; Zhao, Chong; Li, Yongjian; Nie, Mingzhe; Wang, Chunru; Wang, Taishan. An Implanted Paramagnetic Metallofullerene Probe within a Metal–Organic Framework. *Nanoscale* **2018**, *10* (7), 3291–3298. https://doi.org/10.1039/C7NR09420E.

(30) Friščić, Tomislav; Mottillo, Cristina; Titi, Hatem M. Mechanochemistry for Synthesis. *Angew. Chemie Int. Ed.* **2020**, *59* (3), 1018–1029. https://doi.org/10.1002/anie.201906755.

(31) Do, Jean-Louis; Friščić, Tomislav. Mechanochemistry: A Force of Synthesis. *ACS Cent. Sci.* **2017**, *3* (1), 13–19. https://doi.org/10.1021/acscentsci.6b00277.

(32) James, Stuart L.; Adams, Christopher J.; Bolm, Carsten; Braga, Dario; Collier, Paul; Friščić, Tomislav; Grepioni, Fabrizia; Harris, Kenneth D. M.; Hyett, Geoff; Jones, William; et al. Mechanochemistry: Opportunities for New and Cleaner Synthesis. *Chem. Soc. Rev.* **2012**, *41* (1), 413–447. https://doi.org/10.1039/C1CS15171A.

(33) Tan, Davin; Loots, Leigh; Friščić, Tomislav. Towards Medicinal Mechanochemistry: Evolution of Milling from Pharmaceutical Solid Form Screening to the Synthesis of Active Pharmaceutical Ingredients (APIs). *Chem. Commun.* **2016**, *52* (50), 7760–7781. https://doi.org/10.1039/C6CC02015A.

(34) Friščić, Tomislav. Supramolecular Concepts and New Techniques in Mechanochemistry: Cocrystals, Cages, Rotaxanes, Open Metal–Organic Frameworks. *Chem. Soc. Rev.* **2012**, *41* (9), 3493. https://doi.org/10.1039/c2cs15332g.

(35) Do, Jean-Louis; Friščić, Tomislav. Chemistry 2.0: Developing a New, Solvent-Free System of Chemical Synthesis Based on Mechanochemistry. *Synlett* **2017**, *28* (16), 2066–2092. https://doi.org/10.1055/s-0036-1590854.

(36) Boldyreva, Elena. Mechanochemistry of Inorganic and Organic Systems: What Is Similar, What Is Different? *Chem. Soc. Rev.* **2013**, *42* (18), 7719. https://doi.org/10.1039/c3cs60052a.

(37) Stolar, Tomislav; Užarević, Krunoslav. Mechanochemistry: An Efficient and Versatile Toolbox for Synthesis, Transformation, and Functionalization of Porous Metal–Organic Frameworks. *CrystEngComm* **2020**, *22* (27), 4511–4525. https://doi.org/10.1039/D0CE00091D.

(38) Julien, Patrick A.; Mottillo, Cristina; Friščić, Tomislav. Metal–Organic Frameworks Meet Scalable and Sustainable Synthesis. *Green Chem.* **2017**, *19* (12), 2729–2747. https://doi.org/10.1039/C7GC01078H.

(39) Friščić, Tomislav; Halasz, Ivan; Štrukil, Vjekoslav; Eckert-Maksić, Mirjana; Dinnebier, Robert E. Clean and Efficient Synthesis Using Mechanochemistry: Coordination Polymers, Metal-Organic Frameworks and Metallodrugs. *Croat. Chem. Acta* **2012**, *85*, 367–378. https://doi.org/10.5562/cca2014.

(40) Yuan, Wenbing; Garay, Ana Lazuen; Pichon, Anne; Clowes, Rob; Wood, Colin D.; Cooper, Andrew I.; James, Stuart L. Study of the Mechanochemical Formation and Resulting Properties of an Archetypal MOF: Cu3(BTC)2 (BTC = 1,3,5-Benzenetricarboxylate). *CrystEngComm* **2010**, *12* (12), 4063. https://doi.org/10.1039/c0ce00486c.

(41) Klimakow, Maria; Klobes, Peter; Thünemann, Andreas F.; Rademann, Klaus; Emmerling, Franziska. Mechanochemical Synthesis of Metal−Organic Frameworks: A Fast and Facile Approach toward Quantitative Yields and High Specific Surface Areas. *Chem. Mater.* **2010**, *22* (18), 5216–5221. https://doi.org/10.1021/cm1012119.

(42) Stolar, Tomislav; Batzdorf, Lisa; Lukin, Stipe; Žilić, Dijana; Motillo, Cristina; Friščić, Tomislav; Emmerling, Franziska; Halasz, Ivan; Užarević, Krunoslav. In Situ Monitoring of the Mechanosynthesis of the Archetypal Metal–Organic Framework HKUST-1: Effect of Liquid Additives on the Milling Reactivity. *Inorg. Chem.* **2017**, *56* (11), 6599–6608. https://doi.org/10.1021/acs.inorgchem.7b00707.

(43) Julien, Patrick A.; Užarević, Krunoslav; Katsenis, Athanassios D.; Kimber, Simon A. J.; Wang, Timothy; Farha, Omar K.; Zhang, Yuancheng; Casaban, José; Germann, Luzia S.; Etter, Martin; et al. In Situ Monitoring and Mechanism of the Mechanochemical Formation of a Microporous MOF-74 Framework. *J. Am. Chem. Soc.* **2016**, *138* (9), 2929–2932. https://doi.org/10.1021/jacs.5b13038.

(44) Ayoub, Ghada; Karadeniz, Bahar; Howarth, Ashlee J.; Farha, Omar K.; Đilović, Ivica; Germann, Luzia S.; Dinnebier, Robert E.; Užarević, Krunoslav; Friščić, Tomislav. Rational Synthesis of Mixed-Metal Microporous Metal–Organic Frameworks with Controlled Composition Using Mechanochemistry. *Chem. Mater.* **2019**, *31* (15), 5494–5501. https://doi.org/10.1021/acs.chemmater.9b01068.

(45) Užarević, Krunoslav; Wang, Timothy C.; Moon, Su-Young; Fidelli, Athena M.; Hupp, Joseph T.; Farha, Omar K.; Friščić, Tomislav. Mechanochemical and Solvent-Free Assembly of Zirconium-Based Metal–Organic Frameworks. *Chem. Commun.* **2016**, *52* (10), 2133–2136. https://doi.org/10.1039/C5CC08972G.

(46) Karadeniz, Bahar; Howarth, Ashlee J.; Stolar, Tomislav; Islamoglu, Timur; Dejanović, Igor; Tireli, Martina; Wasson, Megan Cathleen; Moon, Su-Young; Farha, Omar K.; Friščić, Tomislav; et al. Benign by Design: Green and Scalable Synthesis of Zirconium UiO-Metal–Organic Frameworks by Water-Assisted Mechanochemistry. *ACS Sustain. Chem. Eng.* **2018**, *6* (11), 15841–15849. https://doi.org/10.1021/acssuschemeng.8b04458.

(47) Fidelli, Athena M.; Karadeniz, Bahar; Howarth, Ashlee J.; Huskić, Igor; Germann, Luzia S.; Halasz, Ivan; Etter, Martin; Moon, Su-Young; Dinnebier, Robert E.;

Stilinović, Vladimir; et al. Green and Rapid Mechanosynthesis of High-Porosity NU- and UiO-Type Metal–Organic Frameworks. *Chem. Commun.* **2018**, *54* (51), 6999–7002. https://doi.org/10.1039/C8CC03189D.

(48) Karadeniz, Bahar; Žilić, Dijana; Huskić, Igor; Germann, Luzia S.; Fidelli, Athena M.; Muratović, Senada; Lončarić, Ivor; Etter, Martin; Dinnebier, Robert E.; Barišić, Dajana; et al. Controlling the Polymorphism and Topology Transformation in Porphyrinic Zirconium Metal–Organic Frameworks via Mechanochemistry. *J. Am. Chem. Soc.* **2019**, *141* (49), 19214–19220. https://doi.org/10.1021/jacs.9b10251.

(49) Beldon, Patrick J.; Fábián, László; Stein, Robin S.; Thirumurugan, A.; Cheetham, Anthony K.; Friščić, Tomislav. Rapid Room-Temperature Synthesis of Zeolitic Imidazolate Frameworks by Using Mechanochemistry. *Angew. Chemie Int. Ed.* **2010**, *49* (50), 9640–9643. https://doi.org/10.1002/anie.201005547.

(50) Bennett, Thomas D.; Cao, Shuai; Tan, Jin Chong; Keen, David A.; Bithell, Erica G.; Beldon, Patrick J.; Friscic, Tomislav; Cheetham, Anthony K. Facile Mechanosynthesis of Amorphous Zeolitic Imidazolate Frameworks. *J. Am. Chem. Soc.* **2011**, *133*, 14546–14549. https://doi.org/10.1021/ja206082s.

(51) Friščić, Tomislav; Halasz, Ivan; Beldon, Patrick J.; Belenguer, Ana M.; Adams, Frank; Kimber, Simon A. J.; Honkimäki, Veijo; Dinnebier, Robert E. Real-Time and in Situ Monitoring of Mechanochemical Milling Reactions. *Nat. Chem.* **2013**, *5* (1), 66–73. https://doi.org/10.1038/nchem.1505.

(52) Souza, Barbara E.; Rudić, Svemir; Titov, Kirill; Babal, Arun S.; Taylor, James D.; Tan, Jin-Chong. Guest–Host Interactions of Nanoconfined Anti-Cancer Drug in Metal–Organic Framework Exposed by Terahertz Dynamics. *Chem. Commun.* **2019**, *55* (27), 3868–3871. https://doi.org/10.1039/C8CC10089F.

(53) Gao, Peng; Shi, Xiaomeng; Xu, Xiaoyan; Wei, Wei. Versatile and Efficient Mechanochemical Synthesis of Crystalline Guest⊂zeolitic Imidazolate Framework Complexes by in Situ Host− Guest Nanoconfinement. *Cryst. Growth Des.* **2018**, *18* (10), 5845–5852. https://doi.org/10.1021/acs.cgd.8b00528.

(54) Orellana-Tavra, Claudia; Marshall, Ross J.; Baxter, Emma F.; Lázaro, Isabel Abánades; Tao, Andi; Cheetham, Anthony K.; Forgan, Ross S.; Fairen-Jimenez, David. Drug Delivery and Controlled Release from Biocompatible Metal–Organic Frameworks Using Mechanical Amorphization. *J. Mater. Chem. B* **2016**, *4* (47), 7697–7707. https://doi.org/10.1039/C6TB02025A.

(55) Glembockyte, Viktorija; Frenette, Mathieu; Mottillo, Cristina; Durantini, Andrés M.; Gostick, Jeff; Štrukil, Vjekoslav; Friščić, Tomislav; Cosa, Gonzalo. Highly Photostable and Fluorescent Microporous Solids Prepared via Solid-State Entrapment of Boron Dipyrromethene Dyes in a Nascent Metal–Organic Framework. *J. Am. Chem. Soc.* **2018**, *140* (49), 16882–16887. https://doi.org/10.1021/jacs.8b09608.

(56) Wei, Tz-Han; Wu, Shi-Hong; Huang, Yi-Da; Lo, Wei-Shang; Williams, Benjamin P.; Chen, Sheng-Yu; Yang, Hsun-Chih; Hsu, Yu-Shen; Lin, Zih-Yin; Chen, Xin-Hua; et al. Rapid Mechanochemical Encapsulation of Biocatalysts into Robust Metal–Organic Frameworks. *Nat. Commun.* **2019**, *10* (1), 5002. https://doi.org/10.1038/s41467-019-12966-0.

(57) Park, K. S.; Ni, Z.; Cote, A. P.; Choi, J. Y.; Huang, R.; Uribe-Romo, F. J.; Chae, H. K.; O'Keeffe, M.; Yaghi, O. M. Exceptional Chemical and Thermal Stability of Zeolitic Imidazolate Frameworks. *Proc. Natl. Acad. Sci.* **2006**, *103* (27), 10186–10191. https://doi.org/10.1073/pnas.0602439103.

(58) Friščić, Tomislav; Reid David, G.; Halasz, Ivan; Stein Robin, S.; Dinnebier Robert, E.; Duer Melinda, J. Ion- and Liquid-Assisted Grinding: Improved Mechanochemical Synthesis of Metal–Organic Frameworks Reveals Salt Inclusion and Anion Templating. *Angew. Chemie Int. Ed.* **2009**, *49*, 712–715. https://doi.org/10.1002/anie.200906583.

(59) Zheng, Haoquan; Zhang, Yuning; Liu, Leifeng; Wan, Wei; Guo, Peng; Nyström, Andreas M.; Zou, Xiaodong. One-Pot Synthesis of Metal-Organic Frameworks with Encapsulated Target Molecules and Their Applications for Controlled Drug Delivery. *J. Am. Chem. Soc.* **2016**, *138* (3), 962–968. https://doi.org/10.1021/jacs.5b11720.

(60) Liédana, Nuria; Galve, Alejandro; Rubio, César; Téllez, Carlos; Coronas, Joaquín. CAF@ZIF-8: One-Step Encapsulation of Caffeine in MOF. *ACS Appl. Mater. Interfaces* **2012**, *4* (9), 5016–5021. https://doi.org/10.1021/am301365h.

(61) Zhao, Yaqian; Ni, Xinjiong; Ye, Sunjie; Gu, Zhi-Guo; Li, Yunxing; Ngai, To. A Smart Route for Encapsulating Pd Nanoparticles into a ZIF-8 Hollow Microsphere and Their Superior Catalytic Properties. *Langmuir* **2020**, *36* (8), 2037–2043. https://doi.org/10.1021/acs.langmuir.9b03731.

(62) Malkar, Radhika S.; Yadav, Ganapati D. Synthesis of Cinnamyl Benzoate over Novel Heteropoly Acid Encapsulated ZIF-8. *Appl. Catal. A Gen.* **2018**, *560* (February), 54–65. https://doi.org/10.1016/j.apcata.2018.04.038.

(63) Katsenis, Athanassios D.; Puškarić, Andreas; Štrukil, Vjekoslav; Mottillo, Cristina; Julien, Patrick A.; Užarević, Krunoslav; Pham, Minh-Hao; Do, Trong-On; Kimber, Simon A. J.; Lazić, Predrag; et al. In Situ X-Ray Diffraction Monitoring of a Mechanochemical Reaction Reveals a Unique Topology Metal-Organic Framework. *Nat. Commun.* **2015**, *6* (1), 6662. https://doi.org/10.1038/ncomms7662.

(64) Akimbekov, Zamirbek; Katsenis, Athanassios D.; Nagabhushana, G. P.; Ayoub, Ghada; Arhangelskis, Mihails; Morris, Andrew J.; Friščić, Tomislav; Navrotsky, Alexandra. Experimental and Theoretical Evaluation of the Stability of True MOF Polymorphs Explains Their Mechanochemical Interconversions. *J. Am. Chem. Soc.* **2017**, *139* (23), 7952–7957. https://doi.org/10.1021/jacs.7b03144.

(65) Brekalo, Ivana; Kane, Christopher M.; Ley, Amanda N.;

Ramirez, Joseph R.; Friščić, Tomislav; Holman, K. Travis. Use of a “Shoe-Last” Solid-State Template in the Mechanochemical Synthesis of High-Porosity RHO-Zinc Imidazolate. *J. Am. Chem. Soc.* **2018**, *140* (32), 10104–10108. https://doi.org/10.1021/jacs.8b05471.

(66) Goel, Anish; Howard, Jack B.; Vander Sande, John B. Size Analysis of Single Fullerene Molecules by Electron Microscopy. *Carbon N. Y.* **2004**, *42* (10), 1907–1915. https://doi.org/10.1016/j.carbon.2004.03.022.

(67) Guan, Jian; Zhong, Xiongwu; Chen, Xiang; Zhu, Xianjun; Li, Panlong; Wu, Jianhua; Lu, Yalin; Yu, Yan; Yang, Shangfeng. Expanding Pore Sizes of ZIF-8-Derived Nitrogen-Doped Microporous Carbon: Via C60 Embedding: Toward Improved Anode Performance for the Lithium-Ion Battery. *Nanoscale* **2018**, *10* (5), 2473–2480. https://doi.org/10.1039/c7nr07829c.

(68) Lukin, Stipe; Tireli, Martina; Stolar, Tomislav; Barišić, Dajana; Blanco, Maria Valeria; di Michiel, Marco; Užarević, Krunoslav; Halasz, Ivan. Isotope Labeling Reveals Fast Atomic and Molecular Exchange in Mechanochemical Milling Reactions. *J. Am. Chem. Soc.* **2019**, *141*, 1212–1216. https://doi.org/10.1021/jacs.8b12149.

(69) Yan, Qiuju; Lin, Yichao; Kong, Chunlong; Chen, Liang. Remarkable CO2/CH4 Selectivity and CO2 Adsorption Capacity Exhibited by Polyamine-Decorated Metal–Organic Framework Adsorbents. *Chem. Commun.* **2013**, *49* (61), 6873. https://doi.org/10.1039/c3cc43352h.

(70) Liang, Jun; Nuhnen, Alexander; Millan, Simon; Breitzke, Hergen; Gvilava, Vasily; Buntkowsky, Gerd; Janiak, Christoph. Encapsulation of a Porous Organic Cage into the Pores of a Metal–Organic Framework for Enhanced CO 2 Separation. *Angew. Chemie Int. Ed.* **2020**, *59* (15), 6068–6073. https://doi.org/10.1002/anie.201916002.

(71) Esken, Daniel; Turner, Stuart; Wiktor, Christian; Kalidindi, Suresh Babu; Van Tendeloo, Gustaaf; Fischer, Roland A. GaN@ZIF-8: Selective Formation of Gallium Nitride Quantum Dots inside a Zinc Methylimidazolate Framework. *J. Am. Chem. Soc.* **2011**, *133* (41), 16370–16373. https://doi.org/10.1021/ja207077u.

(72) Hjorth Larsen, Ask; Jørgen Mortensen, Jens; Blomqvist, Jakob; Castelli, Ivano E.; Christensen, Rune; Dułak, Marcin; Friis, Jesper; Groves, Michael N.; Hammer, Bjørk; Hargus, Cory; et al. The Atomic Simulation Environment—a Python Library for Working with Atoms. *J. Phys. Condens. Matter* **2017**, *29* (27), 273002. https://doi.org/10.1088/1361-648x/aa680e.

(73) Ţucureanu, Vasilica; Matei, Alina; Avram, Andrei Marius. FTIR Spectroscopy for Carbon Family Study. *Crit. Rev. Anal. Chem.* **2016**, *46* (6), 502–520. https://doi.org/10.1080/10408347.2016.1157013.

(74) Schettino, Vincenzo; Pagliai, Marco; Ciabini, Lucia; Cardini, Gianni. The Vibrational Spectrum of Fullerene C 60. *J. Phys. Chem. A* **2001**, *105* (50), 11192–11196. https://doi.org/10.1021/jp012874t.

(75) He, Ming; Yao, Jianfeng; Liu, Qi; Wang, Kun; Chen, Fanyan; Wang, Huanting. Facile Synthesis of Zeolitic Imidazolate Framework-8 from a Concentrated Aqueous Solution. *Microporous Mesoporous Mater.* **2014**, *184*, 55–60. https://doi.org/10.1016/j.micromeso.2013.10.003.

(76) Jafari, Saeed; Ghorbani-Shahna, Farshid; Bahrami, Abdulrahman; Kazemian, Hossein. Effects of Post-Synthesis Activation and Relative Humidity on Adsorption Performance of ZIF-8 for Capturing Toluene from a Gas Phase in a Continuous Mode. *Appl. Sci.* **2018**, *8* (2), 310. https://doi.org/10.3390/app8020310.

(77) Nemes, Laszlo; Ram, Ram S.; Bernath, Peter F.; Tinker, Frank A.; Zumwalt, Michael C.; Lamb, Lowell D.; Huffman, Donald R. Gas-Phase Infrared Emission Spectra of C60 and C70. Temperature-Dependent Studies. *Chem. Phys. Lett.* **1994**, *218* (4), 295–303. https://doi.org/10.1016/0009-2614(93)E1488-3.

(78) Ryder, Matthew R.; Civalleri, Bartolomeo; Bennett, Thomas D.; Henke, Sebastian; Rudić, Svemir; Cinque, Gianfelice; Fernandez-Alonso, Felix; Tan, Jin-Chong. Identifying the Role of Terahertz Vibrations in Metal-Organic Frameworks: From Gate-Opening Phenomenon to Shear-Driven Structural Destabilization. *Phys. Rev. Lett.* **2014**, *113* (21), 215502. https://doi.org/10.1103/PhysRevLett.113.215502.

(79) Leach, Sydney; Vervloet, Michel; Desprès, Alain; Bréheret, Emilienne; Hare, Jonathan P.; John Dennis, T.; Kroto, Harold W.; Taylor, Roger; Walton, David R. M. Electronic Spectra and Transitions of the Fullerene C60. *Chem. Phys.* **1992**, *160* (3), 451–466. https://doi.org/https://doi.org/10.1016/0301-0104(92)80012-K.

(80) Pace, M. D.; Christidis, T. C.; Yin, J. J.; Milliken, J. EPR of a Free Radical in Fullerene, C60: Effect of Molecular Oxygen. *J. Phys. Chem.* **1992**, *96* (17), 6855–6858. https://doi.org/10.1021/j100196a001.

(81) Stankowski, J.; Piekara-Sady, L.; Kempiński, W.; Huminiecki, O.; Sczaniecki, P. B. EPR of Graphite and Fullerenes. *Fuller. Sci. Technol.* **1997**, *5* (6), 1203–1217. https://doi.org/10.1080/15363839708009606.

(82) Paul, Parimal; Kim, Kee-Chan; Sun, Dayong; Boyd, Peter D. W.; Reed, Christopher A. Artifacts in the Electron Paramagnetic Resonance Spectra of C 60 Fullerene Ions: Inevitable C 120 O Impurity. *J. Am. Chem. Soc.* **2002**, *124* (16), 4394–4401. https://doi.org/10.1021/ja011832f.

(83) Konchits, Andriy A.; Shanina, Bela D.; Krasnovyd, Serhii V.; Burya, Alexander I.; Kuznetsova, Olga Yu. Paramagnetic Properties of Fullerene-Derived Nanomaterials and Their Polymer Composites: Drastic Pumping Out Effect. *Nanoscale Res. Lett.* **2017**, *12* (1), 475. https://doi.org/10.1186/s11671-017-2241-3.

(84) Hovmöller, Sven. CRISP: Crystallographic Image Processing on a Personal Computer. *Ultramicroscopy* **1992**, *41* (1), 121–135. https://doi.org/https://doi.org/10.1016/0304-3991(92)90102-P.

(85) Lebedev, O. I.; Millange, F.; Serre, C.; Van Tendeloo, G.; Férey, G. First Direct Imaging of Giant Pores of the Metal−Organic Framework MIL-101. *Chem. Mater.*

2005, *17* (26), 6525–6527. https://doi.org/10.1021/cm051870o.

(86) Wiktor, Christian; Turner, Stuart; Zacher, Denise; Fischer, Roland A.; Tendeloo, Gustaaf Van. Imaging of Intact MOF-5 Nanocrystals by Advanced TEM at Liquid Nitrogen Temperature. *Microporous Mesoporous Mater.* **2012**, *162*, 131–135. https://doi.org/https://doi.org/10.1016/j.micromeso.2012.06.014.

(87) Zhu, Liangkui; Zhang, Daliang; Xue, Ming; Li, Huan; Qiu, Shilun. Direct Observations of the MOF (UiO-66) Structure by Transmission Electron Microscopy. *CrystEngComm* **2013**, *15* (45), 9356–9359. https://doi.org/10.1039/C3CE41122B.

(88) Li, Yuzhang; Wang, Kecheng; Zhou, Weijiang; Li, Yanbin; Vila, Rafael; Huang, William; Wang, Hongxia; Chen, Guangxu; Wu, Gong-Her; Tsao, Yuchi; et al. Cryo-EM Structures of Atomic Surfaces and Host-Guest Chemistry in Metal-Organic Frameworks. *Matter* **2019**, *1* (2), 428–438. https://doi.org/https://doi.org/10.1016/j.matt.2019.06.001.

(89) Zhu, Yihan; Ciston, Jim; Zheng, Bin; Miao, Xiaohe; Czarnik, Cory; Pan, Yichang; Sougrat, Rachid; Lai, Zhiping; Hsiung, Chia-En; Yao, Kexin; et al. Unravelling Surface and Interfacial Structures of a Metal–Organic Framework by Transmission Electron Microscopy. *Nat. Mater.* **2017**, *16* (5), 532–536. https://doi.org/10.1038/nmat4852.

(90) Fairen-Jimenez, D.; Moggach, S. A.; Wharmby, M. T.; Wright, P. A.; Parsons, S.; Düren, T. Opening the Gate: Framework Flexibility in ZIF-8 Explored by Experiments and Simulations. *J. Am. Chem. Soc.* **2011**, *133* (23), 8900–8902. https://doi.org/10.1021/ja202154j.

(91) Haldoupis, Emmanuel; Watanabe, Taku; Nair, Sankar; Sholl, David S. Quantifying Large Effects of Framework Flexibility on Diffusion in MOFs: CH4 and CO2 in ZIF-8. *ChemPhysChem* **2012**, *13* (15), 3449–3452. https://doi.org/10.1002/cphc.201200529.

(92) García-Simón, Cristina; Colomban, Cédric; Çetin, Yarkin Aybars; Gimeno, Ana; Pujals, Míriam; Ubasart, Ernest; Fuertes-Espinosa, Carles; Asad, Karam; Chronakis, Nikos; Costas, Miquel; et al. Complete Dynamic Reconstruction of C60, C70, and (C59N)2 Encapsulation into an Adaptable Supramolecular Nanocapsule. *J. Am. Chem. Soc.* **2020**, *142* (37), 16051–16063. https://doi.org/10.1021/jacs.0c07591.

(93) Gao, Song; Hou, Jingwei; Deng, Zeyu; Wang, Tiesheng; Beyer, Sebastian; Buzanich, Ana Guilherme; Richardson, Joseph J.; Rawal, Aditya; Seidel, Robert; Zulkifli, Muhammad Yazid; et al. Improving the Acidic Stability of Zeolitic Imidazolate Frameworks by Biofunctional Molecules. *Chem* **2019**, *5* (6), 1597–1608. https://doi.org/https://doi.org/10.1016/j.chempr.2019.03.025.

(94) Sun, Chun-Yi; Qin, Chao; Wang, Xin-Long; Yang, Guang-Sheng; Shao, Kui-Zhan; Lan, Ya-Qian; Su, Zhong-Min; Huang, Peng; Wang, Chun-Gang; Wang, En-Bo. Zeolitic Imidazolate Framework-8 as Efficient PH-Sensitive Drug Delivery Vehicle. *Dalt. Trans.* **2012**, *41* (23), 6906–6909. https://doi.org/10.1039/C2DT30357D.

(95) Zhuang, Jia; Kuo, Chun-Hong; Chou, Lien-Yang; Liu, De-Yu; Weerapana, Eranthie; Tsung, Chia-Kuang. Optimized Metal–Organic-Framework Nanospheres for Drug Delivery: Evaluation of Small-Molecule Encapsulation. *ACS Nano* **2014**, *8* (3), 2812–2819. https://doi.org/10.1021/nn406590q.

TOC graphic and caption